Comparative study of the CH4/CO2 adsorption selectivity of activated carbons for biogas upgrading

Deneb Peredo-Mancilla, Camelia Matei Ghimbeu, Bich-Ngoc Ho, Mejdi Jeguirim, Cecile Hort, David Bessieres

Comparative study of the CH_4/CO_2 Adsorption Selectivity of Activated Carbons for Biogas Upgrading

Deneb Peredo-Mancilla[a,b], Camelia Matei Ghimbeu[c], Bich-Ngoc Ho[a,b], Mejdi Jeguirim[c,d], Cecile Hort[b], David Bessieres[a]

[a] *CNRS/Total/Univ Pau & Pays Adour/ E2S UPPA, Laboratoire des Fluides Complexes et Leurs Reservoirs-IPRA, UMRS5150, 64000, Pau, Fr.*
[b] *Univ Pau & Pays Adour/ E2S UPPA, Laboratoire de Thermique, Energetique et Procedes-IPRA, EA1932, 64000, Pau, Fr.*
[c] *Université de Haute-Alsace, Institut de Science des Matériaux de Mulhouse (IS2M), CNRS UMR 7361, F-68100, Mulhouse, Fr.*
[d] *Université de Strasbourg, F-67081 Strasbourg, Fr.*

Abstract

This works provides a new insight on the adsorption of CH_4/CO_2 and its components on carbonaceous materials. The equimolar mixture adsorption isothemrs were obtained for 5 well characterized activated carbons at a temperature of 303 K on the pressure range of 0 to 3 MPa. A higher BET surface area in addition to a narrow pore size distribution centered at a pore size of 0.8 nm resulted in higher CH_4/CO_2 total adsorption capacity. Furthermore, whilst the presence of basic functionalities on the surface of the adsorbents enhanced the adsorption of carbon dioxide, the adsorption selectivity was influenced by both textural and chemical properties of the samples. The selectivity was determined to be higher for carbon ROx 0.8 (selectivity factor of up to 4.7), a microporous steam activated carbon with a mild surface area (1323 $m^2\ g^{-1}$), narrow pore size distribution with an average pore size of 0.84 nm. Higher BET surface areas and average pore sizes resulted in a detriment of the selectivity. In addition, the presence of sulfur surface groups increased resulted in an rise of the selectivity factor.

Keywords: Adsorption, Selectivity, Activated Carbons, Biogas Upgrading

*Deneb Peredo-Mancilla
Email adress: peredo-mancilla.jd@univ-pau.fr

Highlights

- A set of commercial activated carbons was fully characterized by porosimetry analysis, Boehm titration, pH_{PZC}, TPD-MS, DRIFT and TGA.
- The equimolar CH_4/CO_2 mixture adsorption was determined on a wide range of pressure (0-3 MPa) at 303 K.
- Selectivities towards CO_2 are analyzed on terms of the textural and chemical properties.

1. Introduction

The constant increment of global energy demand and the fight against climate change have created the need of turning our energy production systems towards renewable energies [1]. One key alternative to the burning of fossil fuels is the use of biofuels. Derived from biomass, the use of biofuels has environmental benefits such as a decrease in the emissions of CO_2, SO_x and hydrocarbons [2].

Biomethane production via upgrading of biogas is a sustainable source of advanced transport biofuel [3]. The conversion of biogas to biomethane, involves the separation of the methane fraction (40 to 70%) from the carbon dioxide portion (25 to 60%) to obtain a highly purified methane stream (≈95%) that meets the domestic gas pipeline requirements [4, 5, 6]. Compared to other upgrading techniques, the separation of biogas by physical adsorption has the advantages of low investment and operation costs, high efficiency, null production of chemical wastes and no water requirement [7, 8]. It consists in the selective partitioning of carbon dioxide from biogas into an adsorbent material also known as the adsorbent [9]. Adsorbent materials are usually highly porous solids with high specific surface area and developped porosity [10].

Activated carbons (ACs) are commonly used as adsorbents due to their high surface area, developed microporosity, thermal stability, ease of regeneration

and low production cost [11, 12]. They are recognized for their adsorption performance on a variety of separation processes including removal of heavy metals from water [13, 14] and [15], pharmaceutical and organic pollutants removal [16, 17, 18], treatment of flue gas [19, 20], purification of natural gas [21, 22] and upgrading of biogas [23]; [24]. Pure CO_2 gas adsorption has been reported to be influenced by the textural properties of the adsorbents, mainly the narrow micropore volume (<0.7 nm) [25, 26, 27, 28]. Nevertheless, the surface chemistry of the adsorbent is also thought to play a role on the adsorption process ([29, 30]). Liu et al. [31] studied the effect of surface heterogenity on the adsorption process, their results showed an ehacement of CO_2 adsorption when oxygen surface groups such as -OH and -COOH were present, these oxygen functionalities are highly electronegative which allows them to act as basic adsorption sites. Karimi et al. [32] reported an increase on CO_2 adsorption capacity upon removal of surface acidic groups. In fact, due to the acidic properties of carbon dioxide, surface chemistry modification of activated carbons consisting in the addition of basic functionalities is a well studied strategy for the preparation of carbon capture adsorbents [33, 34, 35].

When CO_2 separation of CH_4/CO_2 mixture is concerned, the ideal adsorbent should have a high selectivity provided by different adsorption behavior for the two gases, or in other words it must preferentially adsorb carbon dioxide with the vast majority of methane molecules remaining in the gaseous phase [36]. The two molecules have similar kinetic diameters, 0.330 nm for CO_2 and 0.382 nm for CH_4 which make it very complicated to design kinetic-based adsorbents [37]. However, the two molecules have an important difference of polarity, CO_2 has a quadrupolar moment of $13.4 \cdot 10^{-40}$ cm^2, while CH_4 is a non polar molecule [38]. The presence of polar surface functionalities results in an increased selectivity towards carbon dioxide by means of stronger adsorbate-adsorbant interactions as it was demostrated by Park et al ([39]). They found that a high content of sulfur and potassium on 3 biomass-based activated carbons privileged the adsorption of CO_2. Upon functionalization with NaOH, Fe_2CO_3 of a commercial activated carbon, Castrillon et al. found that the stronger basicity as well as

developed microporosity of the NaOH modified carbon resulted in the highest selectivity [40]. Using molecular dynamics simulations, Wang et al. demonstrated that a low pressure the selectivity is highly influenced by the surface chemistry, whilst at the high pressure region the pore size distribution is the major contributing factor [41].

Although the kind of studies briefly reviewed here are of great importance for the development of new and more efficient biogas upgrading techniques, the bibliography comprising the CO_2 separation from CH_4 by activated carbons remains to this day very limited. The present work explores the role of textural and chemical properties of activated carbons on the CH_4/CO_2 selectivity, by means of the equimolar binary mixture adsorption isotherms for a set of 5 well characterized commercial activated carbons. To the best of our knowledge, this is the first experimental work dealing with the comparison of selectivity values of activated carbons in terms of their textural and surface properties.

2. Materials and Methods

The adsorption selectivity studies were performed on five activated carbons produced by Cabot Corporation (USA). The activated carbons named CNR-115 and CGran are chemically activated with phosphoric acid while GAC 1240, RX 1.5 and Rox 0.8 are physically activated with steam.

2.1. Characterization of the samples

2.1.1. Textural characterization

The textural properties of the activated carbons were obtained by means of nitrogen (N_2) adsorption at 77 K carried out on a Micrometrics ASAP 2000 automatic apparatus with a preparatory step consisting of placing the samples under vacuum for 12 h at 573 K. The BET surface area was obtained from the linear plot in the low pressure region (P/P_0=0.01-0.05) [42]. The total pore volume was calculated from the amount of adsorbed nitrogen at a relative pressure of 0.95. The Dubinin-Radushkevich (DR) equation was used on the

relative pressure range of 10^{-4} to 10^{-2} for obtaining the volume of micropores (pore width w <2 nm) [43], the volume of mesopores (2 nm <w <50 nm) is calculated as the difference between the total pore volume and the micropore volume. This properties can also be found on a previous work of the authors [44].

The pore size distribution was obtained applying the non liquid density functional theory (NLDFT) with the carbon slit pores model to the N_2 adsorption data.

2.1.2. Surface Chemistry characterization

To evaluate the surface chemistry of the activated carbons the temperature programmed desorption TPD profiles were obtained using a "home made" apparatus coupled with mass spectrometry. The temperature of a quartz tube containing 10 g of the sample was increased from 298 to 1223 K at a rate of 2 K per minute, the evolution of carbon monoxide (CO) and carbon dioxide (CO_2) was followed quantitatively using a mass spectrometer (INFINCON Transpector).

In addition, the acid/basic character of the activated carbons was studied by the measurement of the zero charge point pH (pH_{PZC}). For each AC, a quantity of 0.1 g was put in contact with a set of 5 solutions with pH values ranging from 4 to 10 prepared by additions of NaOH 0.1 N or HCl 0.1 N in distillate water. The AC containing solutions were kept under string for 72 h and the pH of the solution was determined by a Denever Instrument model 215 pH meter. The five solutions containing one of the activated carbons had similar final pH values that correspond to the pH_{PZC}. The pH_{PZC} value was refined by following the same protocol using three solutions of pH close to the final values of the first set for each activated carbon.

The presence of acidic and basic oxygen surface groups was studied by the method of Boehm [45]. To calculate the quantity of acidic groups an indirect titration method as described by Schonherr et al. was followed [46]: 200 mg of AC was added to 50 mL of 0.01 N solution of NaOH. The activated carbons

solutions were kept under stirring for 72 h. The supernatant carbons were separated from the solutions by centrifugation followed by decantation. Then, three 10 mL aliquots were taken and 20 mL of 0.01 N hydrochloric acid were added to each sample. Finally, the sodium carbonate Na_2CO_3 0.01 N titration curves were obtained. For each activated carbon-NaOH solution a reference sample containing 50 mL of the NaOH solution was subjected to the same protocol from stirring to titration.

The amount of surface basic functionalities was measured by titration of HCl with Na_2CO_3. The samples containing 50 mL of HCl 0.01 N and 0.200 mg of AC followed the same separation method and treatment time described for basic functionalities. On this case however, direct titration of the 10 mL aliquots by Na_2CO_3 was carried out. The error of the followed Boehm titration protocol is reported to be ∼0.15% of the aliquot volume (10 mL) [46].

DRIFTS (Diffuse Reflectance Infrared Fourier Transform Spectrocopy) analysis of the activated carbons was also performed using an FT-IR spectrometer (Nicolet iS50 FTIR spectrometer, Thermofisher) to indentify the surface functional groups on the activated carbons.

In addition, the thermal stability of the samples was measured by thermogravimetric analysis (TGA) on the temperature range of 303 to 1223 K at a heathing rate of 5°C/min under a nitrogen flow of 100 mL/min using a thermal analyzer TGA/DSC (Mettler toledo).

2.2. CH_4/CO_2 Adsorption experiments

A high pressure manometric device coupled with gas chromatography CG was designed for the calculation of the equimolar CH_4/CO_2 mixture adsorption isotherms, an schematic view of this apparatus can be seen in Figure 1. Its main components are the dosing and adsorption cells (V_{dos} and V_{ads}) (Top Industries, volume: 20.5 cm^3), a recirculation pump (GK-M 24/02, max. flow: 2.8 L/min and max. system pressure: 15 MPa), a manometer (MKS baratron type 121 A, 0.01% uncertainty from vacuum to 3.3 MPa), FID gas chromatograph (Agilent Technologies 7890 A). Isothermal conditions are achieved by a heating wire

controlled by a PID regulator (Eurotherm 3208) and monitored throughout the experiments by two thermocouples placed on each of the cells. A three way valve ($V1$) (Swagelok SS-41GXS2) is placed at the entry of the adsorption system to alternatively allow the entry of the working gas or the extraction of gas samples to be analyzed. Three 2 ways valves ($V2$, $V3$ and $V4$) (Swagelok SS-41GS2) allow the isolation of the dosing cell (V_{dos}) from the adsorption volume (V_{ads}).

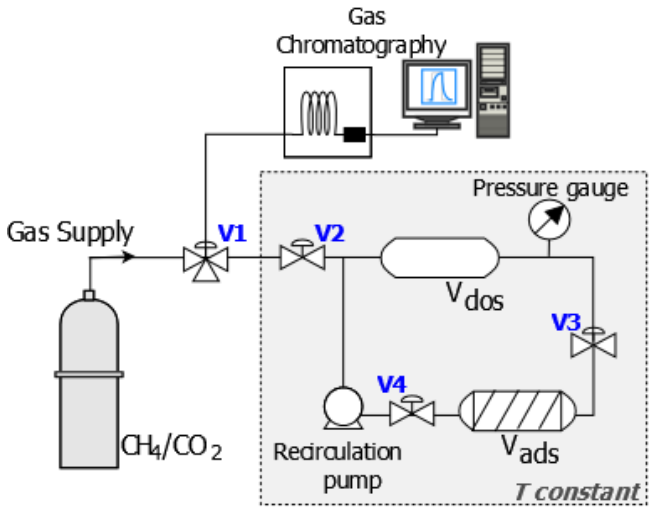

Figure (1) HP adsorption manometric device coupled with gas chromatography.

The procedure starts with the calculation of the accessible volume in the presence of the adsorbent, otherwise known as dead-space volume. To this end, an amount of sample with an adsorption area of at least ∼30 m^2 is placed inside the adsorption volume V_{ads} and cleaned by an 8 h out-gassing process at 373 K under vacuum pressure ($\leq 10^{-2}$ Pa). The dead space volume is obtained by successive helium expansions from the dossing cell V_{dos} to the adsorption cell V_{ads} [47]. Between the dead-space volume calibration and the adsorption measurements, the system is put under vacuum for an additional 4 hours in order to remove any traces of helium.

The protocol for determination of the gas mixture adsorption isotherm follows a mass balance principle. An amount of the CH_4/CO_2 is introduce through valve $V2$ into the dossing cell and the pressure is recorded once the thermal equi-

librium is reached (i.e. constant pressure). The gas is then expanded into the adsorption cell by opening the valves $V3$ and $V4$, homogeneity of the gas during the adsorption process is attained through recirculation of the gas by the recirculation pump, equilibrium is once more achieved and pressure recorded. Valves $V3$ and $V4$ are closed isolating the adsorption cell and a discrete dose of the gas isolated in the dossing section of the system is sent through valve $V1$ to be analyzed by the gas chromatograph.

The total adsorbed amount (n_{ads}) can be then calculated from the difference between the quantity of moles introduced on the dossing cell (n_{dos}) and the amount of moles in the gas phase after adsorption (n_g) (eq. 1).

$$n_{ads} = n_{dos} - n_g \tag{1}$$

From the total adsorbed amount a fraction corresponds to methane and the rest carbon dioxide. Thus, the molar fraction of each gas remaining on the gas phase after the adsorption (y_{CH_4} and y_{CO_2}) needs to be calculated from the integration of the CG peaks. The methane mole fraction in the gas phase is obtained by equation 2.

$$y_{CH_4} = \frac{n_{CH_4,g}}{n_{CH_4,g} + n_{CO_2,g}} \tag{2}$$

The ratio of moles of methane in the adsorbed phase x_{CH_4} can be express also express in the form of a mole fraction (eq. 3)

$$x_{CH_4} = \frac{n_{CH_4,ads}}{n_{CH_4,ads} + n_{CO_2,ads}} \tag{3}$$

Therefore, the quantity of adsorbed moles of methane for the first step of the isotherm is given by multiplication of x_{CH_4} times the total number of adsorbed moles (n_{ads}) as shown by equation 4.

$$n_{CH_4,ads} = x_{CH_4} \times n_{ads} \tag{4}$$

In a similar way, the number of moles of carbon dioxide in the adsorbed phase ($n_{CO_2,ads}$) is expressed by equation 5

$$n_{CO_2,ads} = x_{CO_2} \times n_{ads} \tag{5}$$

For the following steps, the gas in the dossing section of the system is evacuated by the vacuum pump and a new dose of the 50-50% mixture is added to the dossing cell, the pressure is recorded and valves 3 and 4 are opened. The gas molecules that were introduced in the system enter in contact with the gas that was isolated in the adsorption cell on the previous step, recirculation of the gas takes place and a new equilibrium is reached. Therefore, the adsorbed quantity of each gas at a given (i) step of the isotherm can be calculated by equations 6 and 7:

$$n^i_{CH_4,ads} = (\frac{1}{2}n_{dos} + n^{i-1}_g) - (n^i_{CH_4,ads}y^1_{CH_4}) \tag{6}$$

$$n^i_{CO_2,ads} = (\frac{1}{2}n_{dos} + n^{i-1}_g) - (n^i_{CO_2,ads}y^1_{CO_2}) \tag{7}$$

The total adsorbed amount of each gas is calculated by addition of the adsorbed amount on the present step to that of the precedent ones:

$$n_{CH_4,ads} = \sum_i n_{CH_4,ads} \tag{8}$$

and

$$n_{CO_2,ads} = \sum_i n_{CO_2,ads} \tag{9}$$

3. Results And Discussion

3.1. Activated Carbons Characterization

Figure 2 (b) shows the pore size distribution profiles (PSD) for the five activated carbons. A predominance of peaks of under 2 nm can be depicted on this figure, characteristic of microporous materials. Nevertheless, a contribution of mesopores is also present.

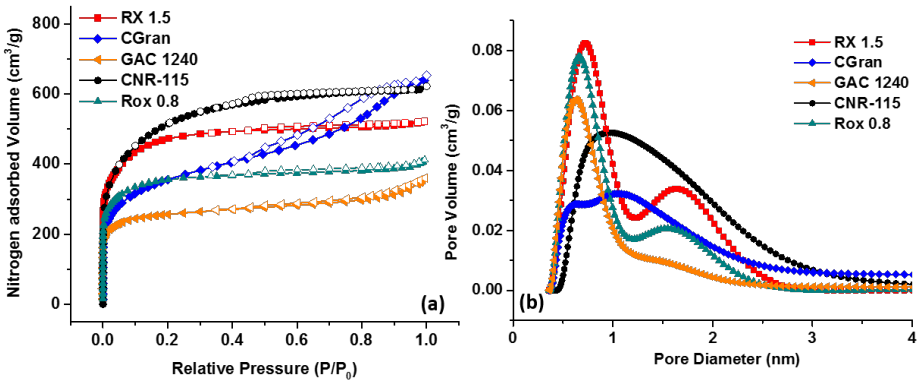

Figure (2) a) Nitrogen adsorption isotherms at 77 K and b) NLDFT pore size distribution of activated carbons RX 1.5, CGran, GAC 1240, CNR-115 and ROx 0.8.

The nitrogen adsorption isotherms on Fig. 2 (a) show type I behavior for activated carbons RX 1.5, GAC 1240, CNR-115 and Rox 0.8 indication of microporous materials. CGran shows a type IV isotherm depicting the presence of an important volume of mesopores. Table 1 shows ACs surface areas (S_{BET}) ranging from 982 (GAC 1240) up to 1714 (CNR-115) in accordance with typical values for carbonaceous materials [48]. The obtained values of micropore volume (V_{micro}) confirm a developed microporosity of the samples. Furthermore, the activated carbons with higher BET surface area, RX 1.5 and CNR-115, also display bigger micropore volumes (0.61 and 0.64 cm^3 $g-1$ respectively). The presence of an important volume of mesopores (V_{meso}) on CGran resulted in the biggest total pore volume V_{tot}, closely followed by CNR-115. Finally, the average pore size (L0) of each sample was calculated using the NLDFT-PSD profiles. The values of L0 ranged from 0.76 (GAC 1240) to 1.10 (CNR-115).

Table (1) Textural Characterization of Activated Carbons

Sample	S_{BET} (m^2 g^{-1})	V_{micro} (cm^3 g^{-1})	V_{meso} (cm^3 g^{-1})	V_{tot} (cm^3 g^{-1})	L0 (nm)
RX 1.5	1683	0.61	0.20	0.81	0.93
CGran	1378	0.45	0.54	0.99	1.00
GAC 1240	982	0.36	0.20	0.56	0.76
CNR-115	1714	0.64	0.31	0.95	1.10
Rox 0.8	1323	0.48	0.16	0.64	0.84

The acid-base properties of the activated carbons were studied by means of their the zero charge point pH (pH_{PZC}) which corresponds to the pH at which the positive and negative surface charges cancel each other. Table 2 displays the obtained values for the aqueous solutions of the activated carbons. A wide range of pH_{PZC} values can be noticed between the activated carbons following the tendency from more to less acidic of CGran > CNR-115 > Gac 1240 > ROx 0.8 > RX 1.5, this trend is closely linked to the activation method used for the preparation of the carbon, with those activated chemically (CGran and CNR-115) showing the highest acidity.

Table (2) Acid-Base character of Activated Carbons

Sample	pH_{PZC}	Total Acid (mmol g^{-1})	Total Basique (mmol g^{-1})
RX 1.5	9.75	0.18	0.73
CGRAN	3.86	1.74	0.01
GAC 1240	8.13	0.18	0.49
CNR-115	6.14	0.49	0.61
ROx 0.8	8.74	0.21	0.61

Moreover, the basic pH_{PZC} values of RX 1.5, ROx 0.8 and GAC 1240 indicates the presence of oxygen functionalities from the families of carbonyles and ethers since they have been reported to create π-electrons rich zones that make the surface acts as a Lewis base [49]. By contrast, activated carbons surface

acidity is thought to be related to the presence of carboxylic acids, lactones and phenols that increase the surface polarity, in the present case a part of acidity may come also from phosforic groups created due to the H_3PO_4 activation agent used [50]. Boehm titration method results (Table 2) confirm the presence of an superior quantity of such functional groups in the acidic pH_{PZC} carbon CGran than on the other activated carbons. Furthermore, activated carbons showing a higher pH_{PZC} presented a bigger quantity of basic oxygen functionalities.

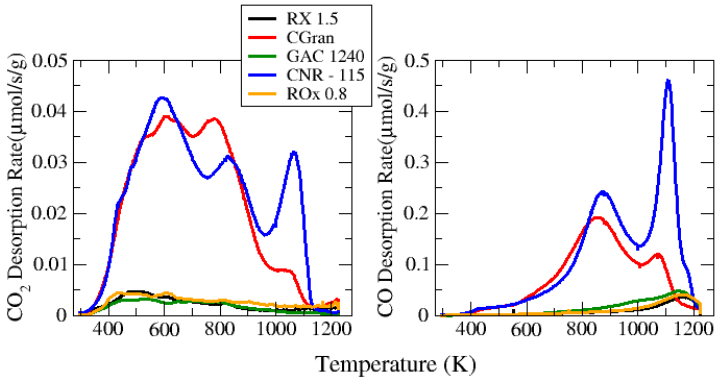

Figure (3) CO_2 and CO TPD desorption profiles for activated carbons RX 1.5, CGran, GAC 1240, CNR-115 and ROx 0.8.

To further investigate the types and quantities of surface groups the TPD-MS profiles were obtained for all of the samples (see Figures 3 and 4). Moreover, the CO and CO_2 TPD-MS profiles show the desorption rates of oxygen surface functionalities upon increasing of the temperature. A considerably bigger amount of oxygen surface groups on activated carbons CGran and CNR-115 can be observed in agreement with the results obtained by the pH_{PZC}. The carbon dioxide desorption profiles of these two activated carbons, indicate the occuring of surface carboxylic groups and lactones functionalities demostrated by the presence of desorption peaks at a temperature below 673 and 923 K respectively. In addition, the peak at 1100 for CNR-115 indicates the presence of thermally stable functionalities such as carbonates. On the other side, the CO desorption profiles of these activated carbons show two peaks, the first one at 900 K cor-

responds to phenol groups, whilst the second one arises from the presence of very thermally stable functionalities such as quinones, ethers, and anhydrides. The remaining activated carbons display a low concentration of oxygen functionalities where the presence of carboxylic acids, ethers and quinones can be depicted. Overall the surface acidic groups quantified by the emission of CO_2 groups are significantly in lower quantities than the basic groups decomposed as CO groups (see Fig. 4). The TPD-MS results are in rather good agreement with the amount of basic and acidic groups determined by Boehm titration (Table 2) except for CGran that shows the presence of basic functionalities that were not detected by the Boehm method, this difference may be originated by limitations of the titration method as reported on the literature [51].

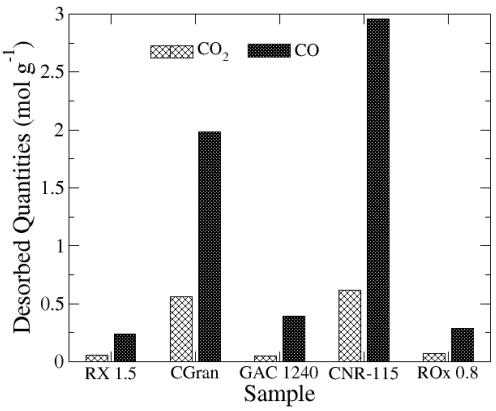

Figure (4) CO_2 and CO_2 TPD total emitted quantities for activated carbons RX 1.5, CGran, GAC 1240, CNR-115 and ROx 0.8 obtained by integration of the desorption peaks.

DRIFTS analysis was performed on the adsorbents to further identify the surface functional groups. Results were gathered in the Figure 5. The ACs presented very heterogeneous surfaces with the presence of both acidic and basic functional groups. Furthermore, a significant difference between the studied adsorbents is observed. For instance, broad peaks detected between 3700 and 3200 cm^{-1} corresponding to hydroxyl functional group can be depicted for all

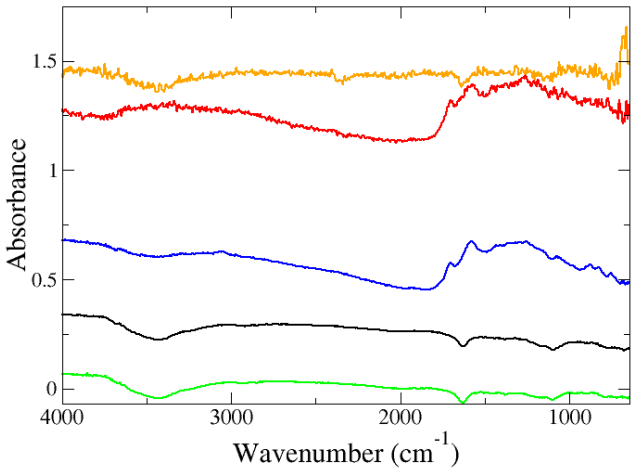

Figure (5) FT-IR spectra for RX 1.5 (black), CGran (red), GAC 1240 (green), CNR-115 (blue) and ROx 0.8 (orange).

the samples except CGran with the peak intensity decreasing significantly in the order of GAC 1240 > RX 1.5 > CNR-115 > ROx 0.8. Simple bands were also detected for all activated carbons, at 1103 cm^{-1} (C-O stretch) and at 880 cm−1 (C-H bend; aromatic structure). This peak is less intense for CNR-115 and CGran ACs. The latter ACs presented a peak between 1500 and 1400 cm^{-1} that could be attributed to the C=C aromatic structure, the DIRFTS profile of this samples is rather distinctive from the others due to its acid character as given by their PH_{PZC} (Table 2) and TPD-MS emmited quantities (Fig. 3), where the presence of carboxylics, lactones and carbonates was depicted. Finally, a vibration peak was detected at the wavenumber gap between 1700 and 1600 cm^{-1} characteristic of the carbonyl, ester and carboxyl C=O stretch on the samples RX 1.5, ROx 0.8 and GAC 1240; this result is in agreement with the basic PH_{PZC} character of the samples and their TPD-MS analysis indicating an important presence of carbonyl and ether functionalities.

The TGA of the ACs shows a high thermal stability for the physically activated samples (RX 1.5, Rox 0.8 and GAC 1240) (see Fig. 6), these samples show

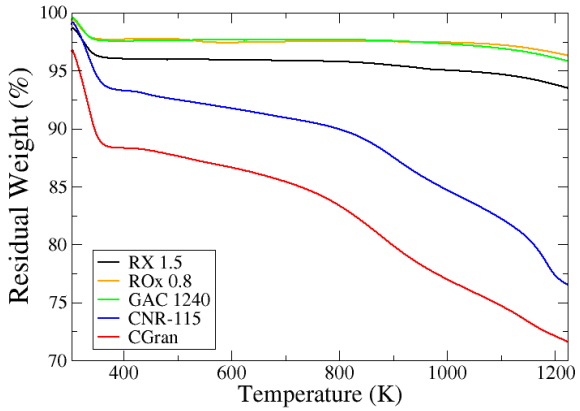

Figure (6) Thermogravimetric analysis (TGA) performed under N_2 flow of activated carbons from 303 to 1223 K: RX 1.5 (black), Cgran (red), GAC 1240 (green), CNR-115 (blue) and ROx 0.8 (orange).

a loss of less than 7% upon temperature increase up to 1223 K. CGran has the lowest thermal stability with a total mass loss of 28% followed by CNR-115 with a mass loss of 22%. An initial mass decay is depicted for the 5 ACs from 303 to ≈ 400 K ascribed to the release of adsorbed water. The drop on weight due to water decreases in the order of: CGran > CNR-115 > RX 1.5 > ROx 0.8≈GAC 1240 in agreement with the H_2O TPS-MS profiles and TPD total emitted quantities of the samples (see Fig. S1 and S3 od supplementary data). After the release of water, the residual weight of CNR-115 and CGran continues to evolve while the others remain stable and in significantly lower amounts. On these two chemically activated carbons, a second stage of thermal decomposition happens up to ≈ 800 K corresponding to the decomposition of oxygen-based functional groups (as highlighted by the TPD-MS). A third stage is depicted on these two carbons above 800 K, the observed cleavage comes from the decomposition of C-H bond resulting in the release of H_2 as demonstrate by the large intense peak of H_2 observed in TPD-MS staring at ≈ 850 K (Fig. S2 of supplementary data).

3.2. CH_4/CO_2 Adsorption experiments

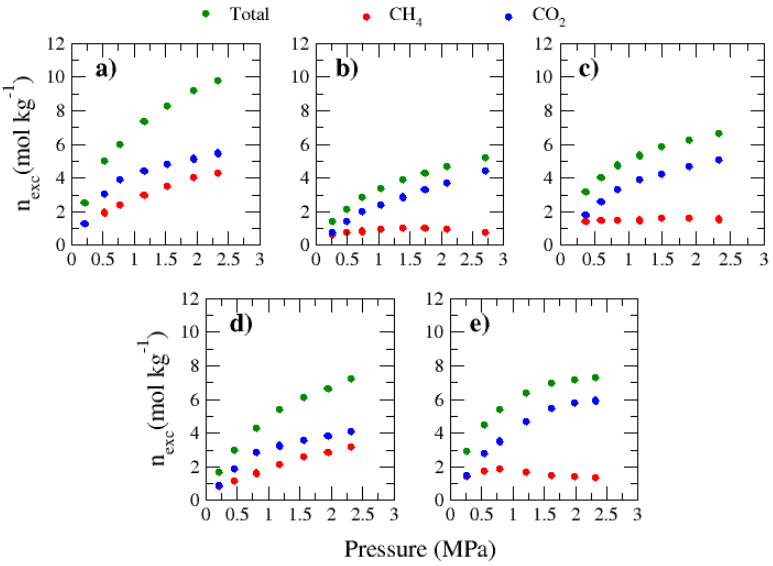

Figure (7) CH_4/CO_2 mixture and individual components in the mixture adsorption at 303 K for activated carbons a) RX 1.5, b) CGran, c) GAC 1240, d) CNR-115 and e) ROx 0.8. (*green: Total, red: CH_4 and blue: CO_2*)

In the context of biogas upgrading, a gas feed containing 50% of CH_4 and 50% of CO_2 was chosen to carry out the adsorption experiments. The adsorption isotherms were obtained for the studied activated carbons at a temperature of 303 K (see Fig. 7, Tables 3-7). The results show a superior carbon dioxide adsorption (blue) compared to that of methane (red) for the five activated carbons. The explanation lays on the difference in polarity of the two probe molecules, while the molecule of carbon monoxide has a high quadrupole moment, methane is a non-polar molecule. Thus, the higher polarizability of CO_2, leads to stronger interactions between the adsorbate and the surface groups of the activated carbons [52]. In addition, an increase of the total adsorbed quantity upon pressure augmentation can also be observed in consistency with typical adsorption behavior on activated carbons.

Table (3) RX 1.5 Adsorption data for each component of the CH_4/CO_2 equimolar mixture at 303 K

RX 1.5								
Pressure (MPa)	$n_{exc}\ CH_4$ (mol kg^{-1})	$n_{exc}\ CO_2$ (mol kg^{-1})	$n_{exc}\ tot$ (mol kg^{-1})	y_{CH4}	y_{CO2}	x_{CH4}	x_{CO2}	F.S.
0,2052	1,2441	1,2622	2,5063	0,5036	0,4964	0,4964	0,5036	1,02
0,5234	1,9505	3,0525	5,0030	0,5155	0,4845	0,3899	0,6101	1,66
0,7737	2,3566	3,8819	5,9741	0,5389	0,4611	0,3777	0,6223	1,92
1,1546	2,9535	4,3765	7,3301	0,5205	0,4795	0,4029	0,5971	1,60
1,5371	3,5132	4,7739	8,2871	0,5008	0,4992	0,4239	0,5761	1,36
1,9547	3,9957	5,1547	9,1503	0,4956	0,5044	0,4367	0,5633	1,26
2,3429	4,2973	5,4857	9,7830	0,4997	0,5003	0,4393	0,5607	1,27

Uncertainties: ΔT=0.2 K, ΔP=0.01 MPa, Δn/n=1%

Table (4) CGran Adsorption data for each component of the CH_4/CO_2 equimolar mixture at 303 K

CGran								
Pressure (MPa)	$n_{exc}\ CH_4$ (mol kg^{-1})	$n_{exc}\ CO_2$ (mol kg^{-1})	$n_{exc}\ tot$ (mol kg^{-1})	y_{CH4}	y_{CO2}	x_{CH4}	x_{CO2}	F.S.
0,2741	0,6353	0,7634	1,3987	0,5458	0,4542	0,4542	0,5458	1,44
0,4953	0,7355	1,4022	2,1376	0,5345	0,4655	0,3441	0,6559	2,18
0,7369	0,8437	1,9722	2,8159	0,5274	0,4726	0,2996	0,7004	2,60
1,0465	0,9544	2,4035	3,3579	0,5196	0,4804	0,2842	0,7158	2,72
1,3864	1,0073	2,8711	3,8784	0,5133	0,4867	0,2597	0,7403	3,00
1,7355	0,9985	3,2955	4,2940	0,5115	0,4885	0,2325	0,7675	3,45
2,0977	0,9558	3,7111	4,6669	0,5095	0,4905	0,2048	0,7952	4,03
2,7128	0,7547	4,4094	5,1641	0,5075	0,4925	0,1461	0,8539	6,02

Uncertainties: ΔT=0.2 K, ΔP=0.01 MPa, Δn/n=1%

Table (5) GAC 1240 Adsorption data for each component of the CH_4/CO_2 equimolar mixture at 303 K

GAC 1240								
Pressure (MPa)	$n_{exc}\ CH_4$ (mol kg^{-1})	$n_{exc}\ CO_2$ (mol kg^{-1})	$n_{exc}\ tot$ (mol kg^{-1})	y_{CH4}	y_{CO2}	x_{CH4}	x_{CO2}	F.S.
0,3701	1,3821	1,7658	3,1478	0,5609	0,4391	0,4391	0,5609	1,63
0,5956	1,4565	2,5465	4,0031	0,5455	0,4545	0,3639	0,6361	2,09
0,8475	1,4567	3,3044	4,7610	0,5356	0,4644	0,3060	0,6940	2,61
1,1765	1,4955	3,8565	5,3519	0,5256	0,4744	0,2794	0,7206	2,85
1,4991	1,6203	4,2295	5,8499	0,5355	0,4645	0,2770	0,7230	3,00
1,8955	1,5965	4,6456	6,2422	0,5105	0,4895	0,2558	0,7442	3,03
2,3293	1,5611	5,0742	6,6353	0,5088	0,4912	0,2353	0,7647	3,36

Uncertainties: ΔT=0.2 K, ΔP=0.01 MPa, $\Delta n/n$=1%

Table (6) CNR-115 Adsorption data for each component of the CH_4/CO_2 equimolar mixture at 303 K

CNR-115								
Pressure (MPa)	$n_{exc}\ CH_4$ (mol kg^{-1})	$n_{exc}\ CO_2$ (mol kg^{-1})	$n_{exc}\ tot$ (mol kg^{-1})	y_{CH4}	y_{CO2}	x_{CH4}	x_{CO2}	F.S.
0,2161	0,8356	0,8515	1,6872	0,5047	0,4953	0,4953	0,5047	1,03
0,4545	1,1345	1,8357	2,9702	0,5245	0,4755	0,3820	0,6180	1,78
0,8097	1,6295	2,8457	4,2752	0,5335	0,4665	0,3641	0,6359	1,99
1,1745	2,0943	3,2647	5,3590	0,5142	0,4858	0,3908	0,6092	1,64
1,5724	2,5574	3,5314	6,0888	0,5005	0,4995	0,4200	0,5800	1,38
1,9456	2,8433	3,8085	6,6517	0,5005	0,4996	0,4274	0,5726	1,34
2,3211	3,1580	4,0862	7,2442	0,4997	0,5003	0,4359	0,5641	1,29

Uncertainties: ΔT=0.2 K, ΔP=0.01 MPa, $\Delta n/n$=1%

Table (7) ROx 0.8 Adsorption data for each component of the CH_4/CO_2 equimolar mixture at 303 K

ROx 0.8								
Pressure (MPa)	$n_{exc}\ CH_4$ (mol kg^{-1})	$n_{exc}\ CO_2$ (mol kg^{-1})	$n_{exc}\ tot$ (mol kg^{-1})	y_{CH4}	y_{CO2}	x_{CH4}	x_{CO2}	F.S.
0,2702	1,4143	1,4886	2,9029	0,5128	0,4872	0,4872	0,5128	1,10
0,5465	1,7155	2,7655	4,4809	0,5257	0,4743	0,3828	0,6172	1,78
0,7958	1,8543	3,5267	5,3810	0,5364	0,4636	0,3446	0,6554	2,20
1,2156	1,6456	4,6947	6,3403	0,5315	0,4685	0,2596	0,7404	3,23
1,6161	1,4644	5,4755	6,9399	0,5305	0,4695	0,2110	0,7890	4,22
1,9901	1,3953	5,7806	7,1759	0,5256	0,4744	0,1944	0,8056	4,59
2,3297	1,3215	5,9427	7,2642	0,5111	0,4889	0,1819	0,8181	4,70

Uncertainties: ΔT=0.2 K, ΔP=0.01 MPa, Δn/n=1%

Carbon dioxide pure gas adsorption on the studied activated carbons was previously found to be directly related to their BET surface area and micropore volume [44]. Here, activated carbons CNR-115 and RX 1.5 present higher adsorption capacities than the rest of activated carbons (see Figure 7) which could indicate influential effect of the BET surface area on the adsorption capacity in agreement with the literature [53, 54]. The calculation of the BET surface area provides an estimation of available physisorption sites, thus explaining the higher adsorption of this carbons. Nonetheless, it can be seen that even though the adsorption capacity of carbon dioxide is favored, their methane adsorption is also important, an unwanted behavior for the separation of these two gases. Furthermore, when adsorption competition between the two gases is present, other factors seem to play an important role as evidenced upon comparison of the adsorption isotherms of CGran and ROx 0.8 (Fig 7 (b) and (e)). The two samples have very similar surface areas (1378 and 1323 $m^2\ g^{-1}$) and micropore volume (0.45 and 0.48 $cm^3\ g^{-1}$) but nevertheless the CO_2 and CH_4/CO_2 total adsorption are significantly more important on ROx 0.8. One possible explanation for the difference in adsorption capacity of these 2 activated carbons

relays on tn their pore size distribution, ROx 0.8 presents a more narrow pore distribution with a typical pore size close to 0.7 nm, meanwhile CGran present a wider pore distribution centered at $\approx$ 1 nm. In fact, a narrow pore distribution with an average pore size between 0.7 and 0.8 nm has been reported to be optimal for adsorption of both methane and carbon dioxide [55, 27]. Another explanation lays on the surface chemistry of the samples. Xue et al. [56] found that the surface chemistry of the adsorbent also affects the total adsorbed quantity and individual components adsorption of gas mixtures. As aforementioned CGran has the lowest pH_{PZC} and the highest quantity of acidic surface functionalities, with CO_2 behaving as a Lewis acid, the result is the decrease on the adsorbed amount of the equimolar mixture. This is also a valid explanation for the significant decrease on the CNR-115 adsorption compared to RX 1.5.

The study of the equimolar mixture adsorption, allows to determined the role of the adsorbent properties on the adsorption process by establishing competition conditions on equal grounds for the two gases. However, attention must be made to the gas feed composition for industrial applications of adsorption separation of biogas using activated carbons. The literature review, indicates that a higher concentrations of methane (i. ex. 75% CH_4-25% CO_2 mixture) leads to lower adsorbed quantities of carbon dioxide than methane and on the opposite case (25% CH_4-75% CO_2) the adsorption of methane drops to a point where up to 90% of the adsorbed gas is carbon dioxide [57, 58, 59].

The individual components adsorption from the equimolar mixture of AC ROx 0.8 is compared with bibliographic data of activated carbons on Figure 8, this sample was chosen due to its low adsorption of methane (< 2 mol kg^{-1}) and high adsorption of carbon dioxide (up to 6 mol kg^{-1}). As this figure shows most of the data found on the literature reported adsorption values at low pressure and up to 1 MPa. Ecosorb, a reference activated carbon presents the highest adsorption of CO_2 found in the literature, however it has the disadvantage of a high adsorption of methane at high pressure, which indicates a low capacity of separation [60]. The rest of the activated carbons present very similar adsorption values of both components of the mixture, with the exception of CS H_2O that

has lower adsorption values atributed to its low surface area (998 m^2 g^{-1}) [52, 58, 61].

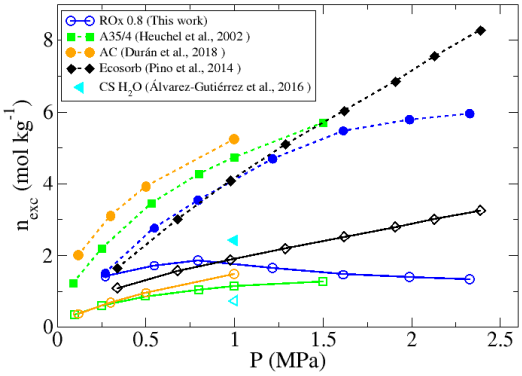

Figure (8) Comparison of CH_4/CO_2 adsorption of activated carbon ROx 0.8 with reported values on the literature, filled symbols with dashed lines correspond to the adsorption of CO_2 while empty symbols with solid lines correspond to the adsorption of CH_4 from the equimolar mixture. The lines between the data are added for visualization purposes.

In addition to the adsorbed quantity, the adsorbent preference for carbon dioxide over methane is a very important indicator of the performance on the CH_4/CO_2 separation. The selectivity factor is then defined by equation 10,

$$S_{ij} = \frac{y_i/y_j}{x_i/x_j} \tag{10}$$

Where $S_{i/j}$ is the selctivity factor for the i/j separation. On this equation, i stands for CH_4 and j for CO_2, the CH_4 and CO_2 bulk phase mole fractions are represented by y_i and y_j and the adsorbed mole fractions by x_i and x_j.

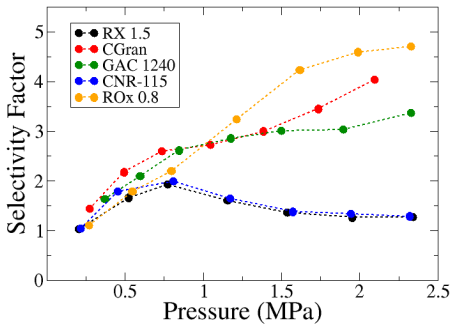

Figure (9) CH_4/CO_2 selectivity factor at 303 K for activated carbons: RX 1.5 (black), CGran (red), GAC 1240 (green), CNR-115 (blue) and ROx 0.8 (yellow). Dashed lines are added for visualization purposes

Figure 9 presents the selectivity factor obtained for the activated carbons over the studied pressure range. The obtained selectivity factors of the set of activated carbons indicate a preferential adsorption of CO_2 over CH_4 (i.e. selectivity factor >1).

On this figure, an enhancement of the selectivity of the activated carbons with increasing of the gas pressure can be observed for GAC 1240, CGran and ROx 0.8, explained by the shape of the adsorption isotherms, the adsorbed gas quantity grows steeper for carbon dioxide than for methane for these ACs. The rise in selectivity with pressure is also reported to be related to intermolecular cooperative (energetic) effects [62]. At small pressures the interaction of the gas molecules with the adsorbent is predominant, thus the CO_2 molecules are preferentially adsorbed on the pores surface due to stronger adsorbent-adsorbate interactions. Activated carbons RX 1.5 and CNR-115 present a more developed microporosity with pores under 1 nm (Fig. 2), at low pressure the flat and smaller carbon dioxide molecules can easily diffuse in the micropores, at higher pressures, methane molecules are compressed resulting in an increase of their concentration on the adsorbed phase and consequently in a lower selectivity factor. In addition, their high surface area also lowers their selectivity by a weakening of the influence of the adsorbent-adsorbate interaction strength

upon the overall adsorption process [41]. The highest selectivity factor at high pressure was found for the activated carbon ROx 0.8 an activated carbon with a mild surface area (1323 m^2 g^{-1}) and the lowest mesopore volume (0.16 cm^3) between the activated carbons. In contrast with the other samples, this carbon showed an important presence of sulfur surface groups during the TPD-MS analysis (SO_2 total desorbed quantity: 0.24 mol g^{-1}), the existence of S-based surface groups has been found to increase the surface basicity thus resulting in higher CO_2 adsorption and CH_4/CO_2 selectivity [63, 64].

The surface chemistry of the activated carbons have been reported to have an effect on the selectivity [41, 65], in particular, the presence of basic functionalities is reported to increase selectivity on the low pressure range. In this work, no direct relationship between the presence of such groups and the selectivity was found, instead, the selectivity of the studied activated carbons seems to be given by a mixture of factors including micropore volume, pore size, surface area and surface chemistry. With selectivity been enhanced by small surface area, narrow pore size distribution at an optimal average pore size of 0.8 nm and the presence of basic surface functionalities.

The commercial upgrading of biogas commonly uses carbon base adsorbents such as activated carbons, with reported CH_4/CO_2 selectivity values between 2 and 4 [66]. On this regard, Table 8 displays the selectivity values of different carbonaceous materials reported on the literature at 1 MPa and initial CO_2 molar concentration $Y(CO_2)$ near to 50%. The selectivity values obtained in this work are comparable to those in the literature for carbonaceous materials under similar conditions.

Table (8) Comparison of CH_4/CO_2 selectivity of carbonaceous materials at 1 MPa

Sample	Y(CO_2)	Selectivity	T (K)	Reference
WV1050	47.3	5.2	303	[67]
Norit R1	42	2.7	298	[68]
Honeycomb monoliths	50	2.0	299	[69]
A35/4	50	3.4	293	[58]
Ordered mesoporous carbon	50	3.0	298	[70]
Desorex K43-Na	45	2.1	298	[40]
RX 1.5	50	1.7	303	This work
CGRAN	50	2.7	303	This work
GAC 1240	50	2.7	303	This work
CNR-115	50	1.8	303	This work
ROx 0.8	50	2.5	303	This work

4. Conclusions

The present work provides a comprehensive analysis of the mayor factors influencing the adsorption capacity and selectivity of the carbon dioxide and methane mixture onto activated carbons. To this end, the equimolar CH_4/CO_2 binary mixture adsorption isotherms were obtained for a set of five activated carbons on the pressure range of 0 to 3 MPa. The presence of basic functionalities had a possitive effect on the carbon dioxide adsorption capacity. In addition, higher surface area resulted in increased mixture adsorption capacity, however, it's effect was detrimental for the gas separation process, i.e. the adsorption capacity of methane was also increased reducing the adsorbent selectivity. Overall, a mix of textural and chemical properties was found to be responsible the selectivity of an adsorbent.

5. Acknowledgement

Deneb Peredo is grateful to CONACyT for the fellowship 293897 to pursue her PhD degree. The authors would also like to acknowledge Bénédicte Réty for

her assistance with the TPD-MS measurements. The authors acknowledge the institute CARNOT ISIFoR for the given financing through the project Epur-BioAdStoc.

6. References

1. Yang N, Wang R. Sustainable technologies for the reclamation of greenhouse gas CO_2. *J Clean Prod* 2015;103:784–92. URL: http://dx.doi.org/10.1016/j.jclepro.2014.10.025. doi:10.1016/j.jclepro.2014.10.025.

2. Shuba ES, Kifle D. Microalgae to biofuels: Promising' alternative and renewable energy, review. *Renew Sust Energ Rev* 2018;81(May 2017):743–55. doi:10.1016/j.rser.2017.08.042.

3. Tabassum MR, Xia A, Murphy JD. Biomethane production from various segments of brown seaweed. *Energ Convers Manage* 2018;174(July):855–62. URL: https://doi.org/10.1016/j.enconman.2018.08.084. doi:10.1016/j.enconman.2018.08.084.

4. Pellegrini LA, De Guido G, Langé S. Biogas to liquefied biomethane via cryogenic upgrading technologies. *Renew Energy* 2018;124:75–83. doi:10.1016/j.renene.2017.08.007.

5. Augelletti R, Conti M, Annesini MC. Pressure swing adsorption for biogas upgrading. A new process configuration for the separation of biomethane and carbon dioxide. *J Clean Prod* 2016;140:1390–8. URL: http://dx.doi.org/10.1016/j.jclepro.2016.10.013. doi:10.1016/j.jclepro.2016.10.013.

6. Jiang Y, Ling J, Xiao P, He Y, Zhao Q, Chu Z, Liu Y, Li Z, Webley PA. Simultaneous biogas purification and CO2capture by vacuum swing adsorption using zeolite NaUSY. *Chemical Engineering Journal* 2018;334(November 2017):2593–602. URL: https://doi.org/10.1016/j.cej.2017.11.090. doi:10.1016/j.cej.2017.11.090.

7. Zacharia R, Gomez LF, Chahine R, Cossement D, Benard P. Thermodynamics and kinetics of CH_4/CO_2 binary mixture separation by metal-organic frameworks from isotope exchange and adsorption breakthrough. *Micropor Mesopor Mat* 2018;263(December 2017):165–72. URL: https://doi.org/10.1016/j.micromeso.2017.12.011. doi:10.1016/j.micromeso.2017.12.011.

8. Angelidaki I, Treu L, Tsapekos P, Luo G, Campanaro S, Wenzel H, Kougias PG. Biogas upgrading and utilization: Current status and perspectives. *Biotechnol Adv* 2018;36(2):452–66. URL: https://doi.org/10.1016/j.biotechadv.2018.01.011. doi:10.1016/j.biotechadv.2018.01.011.

9. Álvarez-Gutiérrez N, Gil MV, Rubiera F, Pevida C. Simplistic approach for preliminary screening of potential carbon adsorbents for CO_2 separation from biogas. *J CO2 Util* 2018;28(September):207–15. URL: https://doi.org/10.1016/j.jcou.2018.10.001. doi:10.1016/j.jcou.2018.10.001.

10. Miltner M, Makaruk A, Harasek M. Review on available biogas upgrading technologies and innovations towards advanced solutions. *J Clean Prod* 2017;161(2017):1329–37. URL: http://dx.doi.org/10.1016/j.jclepro.2017.06.045. doi:10.1016/j.jclepro.2017.06.045.

11. Zheng Y, Li Q, Yuan C, Tao Q, Zhao Y, Zhang G, Liu J. Influence of temperature on adsorption selectivity: Coal-based activated carbon for CH 4 enrichment from coal mine methane. *Powder Technol* 2019;347:42–9. URL: https://doi.org/10.1016/j.powtec.2019.02.042. doi:10.1016/j.powtec.2019.02.042.

12. Feroldi M, Neves AC, Borba CE, Alves HJ. Methane storage in activated carbon at low pressure under different temperatures and flow rates of charge. *J Clean Prod* 2018;172:921–6. URL: https://doi.org/10.1016/j.jclepro.2017.10.247. doi:10.1016/j.jclepro.2017.10.247.

13. Valentín-Reyes J, García-Reyes RB, García-González A, Soto-Regalado E, Cerino-Córdova F. Adsorption mechanisms of hexavalent chromium

from aqueous solutions on modified activated carbons. *J Environ Manage* 2019;236(July 2016):815–22. URL: https://doi.org/10.1016/j.jenvman.2019.02.014. doi:10.1016/j.jenvman.2019.02.014.

14. Karnjanakom S, Maneechakr P. Adsorption behaviors and capacities of Cr(VI) onto environmentally activated carbon modified by cationic (HDTMA and DDAB) surfactants. *J Mol Struct* 2019;1186:80–90. URL: https://doi.org/10.1016/j.molstruc.2019.03.022. doi:10.1016/j.molstruc.2019.03.022.

15. Kyzas GZ, Bomis G, Kosheleva RI, Efthimiadou EK, Favvas EP, Kostoglou M, Mitropoulos AC. Nanobubbles effect on heavy metal ions adsorption by activated carbon. *Chem Eng J* 2019;356(September 2018):91–7. URL: https://doi.org/10.1016/j.cej.2018.09.019. doi:10.1016/j.cej.2018.09.019.

16. Delgado N, Capparelli A, Navarro A, Marino D. Pharmaceutical emerging pollutants removal from water using powdered activated carbon: Study of kinetics and adsorption equilibrium. *J Environ Manage* 2019;236(February):301–8. URL: https://doi.org/10.1016/j.jenvman.2019.01.116. doi:10.1016/j.jenvman.2019.01.116.

17. Pamphile N, Xuejiao L, Guangwei Y, Yin W. Synthesis of a novel core-shell-structure activated carbon material and its application in sulfamethoxazole adsorption. *J Hazard Mater* 2019;368(October 2018):602–12. doi:10.1016/j.jhazmat.2019.01.093.

18. Durán-Jiménez G, Hernández-Montoya V, Montes-Morán MA, Bonilla-Petriciolet A, Rangel-Vázquez NA. Adsorption of dyes with different molecular properties on activated carbons prepared from lignocellulosic wastes by Taguchi method. *Micropor Mesopor Mat* 2014;199:99–107. doi:10.1016/j.micromeso.2014.08.013.

19. Lopez-Anton MA, Rumayor M, Díaz-Somoano M, Martínez-Tarazona MR.

Influence of a CO_2-enriched flue gas on mercury capture by activated carbons. *Chem Eng J* 2015;262:1237–43. URL: http://dx.doi.org/10.1016/j.cej.2014.10.088. doi:10.1016/j.cej.2014.10.088.

20. Wawrzyńczak D, Majchrzak-Kucęba I, Srokosz K, Kozak M, Nowak W, Zdeb J, Smółka W, Zajchowski A. The pilot dual-reflux vacuum pressure swing adsorption unit for CO_2 capture from flue gas. *Sep Purif Technol* 2019;209(March 2018):560–70. doi:10.1016/j.seppur.2018.07.079.

21. Aguiar MF, Coelho GL. Adsorption of sulfur compounds from natural gas by different adsorbents and desorption using supercritical CO_2. *J Environ Chem Eng* 2017;5(5):4353–64. URL: http://dx.doi.org/10.1016/j.jece.2017.07.079. doi:10.1016/j.jece.2017.07.079.

22. Ghanbari S, Niu CH. Characteristics of oat hull based biosorbent for natural gas dehydration in a PSA process. *J Nat Gas Sci Eng* 2019;61(November 2018):320–32. URL: https://doi.org/10.1016/j.jngse.2018.11.014. doi:10.1016/j.jngse.2018.11.014.

23. Vivo-Vilches JF, Pérez-Cadenas AF, Maldonado-Hódar FJ, Carrasco-Marín F, Faria RP, Ribeiro AM, Ferreira AF, Rodrigues AE. Biogas upgrading by selective adsorption onto CO_2 activated carbon from wood pellets. *J Environ Chem Eng* 2017;5(2):1386–93. URL: http://dx.doi.org/10.1016/j.jece.2017.02.015. doi:10.1016/j.jece.2017.02.015.

24. Mamun MRA, Karim MR, Rahman MM, Asiri AM, Torii S. Methane enrichment of biogas by carbon dioxide fixation with calcium hydroxide and activated carbon. *J Taiwan Inst Chem E* 2016;58:476–81. doi:10.1016/j.jtice.2015.06.029.

25. Montagnaro F, Silvestre-Albero A, Silvestre-Albero J, Rodríguez-Reinoso F, Erto A, Lancia A, Balsamo M. Post-combustion CO_2 adsorption on activated carbons with different textural properties. *Micropor Mesopor Mat* 2015;209:157–64. URL: http://dx.doi.org/10.1016/j.micromeso.2014.09.037. doi:10.1016/j.micromeso.2014.09.037.

26. Serafin J, Narkiewicz U, Morawski AW, Wróbel RJ, Michalkiewicz B. Highly microporous activated carbons from biomass for CO2capture and effective micropores at different conditions. *J CO2 Util* 2017;18:73–9. doi:10.1016/j.jcou.2017.01.006.

27. Presser V, McDonough J, Yeon SH, Gogotsi Y. Effect of pore size on carbon dioxide sorption by carbide derived carbon. *Energy Environ Sci* 2011;4(8):3059. URL: http://xlink.rsc.org/?DOI=c1ee01176f. doi:10.1039/c1ee01176f. arXiv:caps 17.

28. Yin G, Liu Z, Liu Q, Wu W. The role of different properties of activated carbon in CO2adsorption. *Chem Eng J* 2013;230:133–40. URL: http://dx.doi.org/10.1016/j.cej.2013.06.085. doi:10.1016/j.cej.2013.06.085.

29. Peredo-Mancilla D, Ghouma I, Hort C, Bessieres D, Matei Ghimbeu C. Gas storage. In: *Char and Carbon Materials Derived from Biomass*. Amsterdam: Elsevier Inc. ISBN 978-0-12-814893-8; 2019:341–82. doi:https://doi.org/10.1016/C2017-0-02406-0.

30. Chatti R, Bansiwal AK, Thote JA, Kumar V, Jadhav P, Lokhande SK, Biniwale RB, Labhsetwar NK, Rayalu SS. Amine loaded zeolites for carbon dioxide capture: Amine loading and adsorption studies. *Micropor Mesopor Mat* 2009;121(1-3):84–9. URL: http://dx.doi.org/10.1016/j.micromeso.2009.01.007. doi:10.1016/j.micromeso.2009.01.007.

31. Liu Y, Wilcox J. Effects of surface heterogeneity on the adsorption of CO_2 in microporous carbons. *Environ Sci Technol* 2012;46(3):1940–7. doi:10.1021/es204071g.

32. Karimi M, Silva JA, Gonçalves CN, Diaz De Tuesta JL, Rodrigues AE, Gomes HT. CO_2 Capture in Chemically and Thermally Modified Activated Carbons Using Breakthrough Measurements: Experimental and Modeling Study. *Ind Eng Chem Res* 2018;57(32):11154–66. doi:10.1021/acs.iecr.8b00953.

33. Meng LY, Park SJ. One-pot synthetic method to prepare highly N-doped nanoporous carbons for CO_2 adsorption. *Mater Chem Phys* 2014;143(3):1158–63. URL: http://dx.doi.org/10.1016/j.matchemphys.2013.11.016. doi:10.1016/j.matchemphys.2013.11.016.

34. Yadavalli G, Lei H, Wei Y, Zhu L, Zhang X, Liu Y, Yan D. Carbon dioxide capture using ammonium sulfate surface modified activated biomass carbon. *Biomass Bioenergy* 2017;98:53–60. URL: http://dx.doi.org/10.1016/j.biombioe.2017.01.015. doi:10.1016/j.biombioe.2017.01.015.

35. Caglayan BS, Aksoylu AE. CO_2 adsorption on chemically modified activated carbon. *J Hazard Mater* 2013;252-253:19–28. URL: http://dx.doi.org/10.1016/j.jhazmat.2013.02.028. doi:10.1016/j.jhazmat.2013.02.028.

36. Zhao Y, Liu X, Han Y. Microporous carbonaceous adsorbents for CO_2 separation via selective adsorption. *RSC Adv* 2015;5(38):30310–30. URL: http://dx.doi.org/10.1039/C5RA00569H. doi:10.1039/c5ra00569h.

37. Kennedy DA, Tezel FH. Cation exchange modification of clinoptilolite Screening analysis for potential equilibrium and kinetic adsorption separations involving methane, nitrogen, and carbon dioxide. *Micropor Mesopor Mat* 2018;262(July 2017):235–50. URL: https://doi.org/10.1016/j.micromeso.2017.11.054. doi:10.1016/j.micromeso.2017.11.054.

38. D'Alessandro DM, Smit B, Long JR. Carbon dioxide capture: Prospects for new materials. *Angew Chem Int Ed Engl* 2010;49(35):6058–82. doi:10.1002/anie.201000431.

39. Park J, Attia NF, Jung M, Lee ME, Lee K, Chung J, Oh H. Sustainable nanoporous carbon for CO_2, CH_4, N_2, H_2 adsorption and CO2/CH4 and CO2/N2 separation. *Energy* 2018;158:9–16. URL: https://doi.org/10.1016/j.energy.2018.06.010. doi:10.1016/j.energy.2018.06.010.

40. Castrillon MC, Moura KO, Alves CA, Bastos-Neto M, Azevedo DC, Hofmann J, Möllmer J, Einicke WD, Gläser R. CO_2 and H_2S Removal from CH4-Rich Streams by Adsorption on Activated Carbons Modified with K_2CO_3, NaOH, or Fe_2O_3. *Energy and Fuels* 2016;30(11):9596–604. doi:10.1021/acs.energyfuels.6b01667.

41. Wang S, Lu L, Wu D, Lu X, Cao W, Yang T, Zhu Y. Molecular Simulation Study of the Adsorption and Diffusion of a Mixture of CO2/CH4 in Activated Carbon: Effect of Textural Properties and Surface Chemistry. *J Chem Eng Data* 2016;61(12):4139–47. doi:10.1021/acs.jced.6b00554.

42. Brunauer S, Emmett PH, Teller E. Adsorption of Gases in Multimolecular Layers. *J Am Chem Soc* 1938;60(2):309–19. doi:10.1021/ja01269a023. arXiv:arXiv:1011.1669v3.

43. Dubinin MM, Radushkevich L. *Doklady akademii nauk SSSR* 1947;55:331.

44. Peredo-Mancilla D, Hort C, Jeguirim M, Ghimbeu CM, Limousy L, Bessieres D. Experimental Determination of the CH_4 and CO_2 Pure Gas Adsorption Isotherms on Different Activated Carbons. *J Chem Eng Data* 2018;63:3027–34. URL: http://pubs.acs.org/doi/10.1021/acs.jced.8b00297. doi:10.1021/acs.jced.8b00297.

45. Boehm HP. Some aspects of the surface chemistry of carbon blacks and other carbons. *Carbon* 1994;32(5):759–69. doi:10.1016/0008-6223(94)90031-0.

46. Schönherr J, Buchheim JR, Scholz P, Adelhelm P. Boehm Titration Revisited (Part I): Practical Aspects for Achieving a High Precision in Quantifying Oxygen-Containing Surface Groups on Carbon Materials. *C* 2018;4(2):21. doi:10.3390/c4020021.

47. Bessières D, Lafitte T, Daridon JL, Randzio SL. High pressure thermal expansion of gases: Measurements and calibration. *Thermochim Acta* 2005;428(1-2):25–30. doi:10.1016/j.tca.2004.09.020.

48. Chen Y, Zhou Lj, Hong Yz, Cao F, Li L, Li Jb. Preparation of high-surface-area activated carbon from coconut shell fibers. *Carbon* 2010;48(10):3005. URL: http://linkinghub.elsevier.com/retrieve/pii/S0008622310002241. doi:10.1016/j.carbon.2010.03.059.

49. Moreno-Castilla C. Adsorption of organic molecules from aqueous solutions on carbon materials. *Carbon* 2004;42(1):83–94. doi:10.1016/j.carbon.2003.09.022.

50. Ghimbeu CM, Gadiou R, Dentzer J, Schwartz D, Vix-Guterl C. Influence of surface chemistry on the adsorption of oxygenated hydrocarbons on activated carbons. *Langmuir* 2010;26(24):18824–33. doi:10.1021/la103405j.

51. Kalijadis AM, Vukčević MM, Jovanović ZM, Laušević ZV, Laušević MD. Characterisation of surface oxygen groups on different carbon materials by the Boehm method and temperature-programmed desorption. *Journal of the Serbian Chemical Society* 2011;76(5):757–68. doi:10.2298/JSC091224056K.

52. Álvarez-Gutiérrez N, Gil MV, Rubiera F, Pevida C. Adsorption performance indicators for the CO_2/CH_4 separation: Application to biomass-based activated carbons. *Fuel Processing Technology* 2016;142:361–9. URL: http://dx.doi.org/10.1016/j.fuproc.2015.10.038. doi:10.1016/j.fuproc.2015.10.038.

53. Boshir Ahmed M, Abu Hasan Johir M, Zhou JL, Hao Ngo H, Duc Nghiem L, Richardson C, Ali Moni M, Bryant MR. Activated carbon preparation from biomass feedstock: Clean production and carbon dioxide adsorption. *J Clean Prod* 2019;225:405–13. URL: https://doi.org/10.1016/j.jclepro.2019.03.342. doi:10.1016/j.jclepro.2019.03.342.

54. Singh J, Basu S, Bhunia H. Dynamic CO_2 adsorption on activated carbon adsorbents synthesized from polyacrylonitrile (PAN): Kinetic and isotherm studies. *Micropor Mesopor Mat* 2019;280(November 2018):357–66. URL:

https://doi.org/10.1016/j.micromeso.2019.02.031. doi:10.1016/j.micromeso.2019.02.031.

55. Lozano-Castelló D, Cazorla-Amorós D, Linares-Solano A, Quinn DF. Influence of pore size distribution on methane storage at relatively low pressure: Preparation of activated carbon with optimum pore size. *Carbon* 2002;40(7):989–1002. doi:10.1016/S0008-6223(01)00235-4.

56. Xue CL, Cheng WP, Hao WM, Hong M, Li RF. CH4/N2 Adsorptive Separation on Zeolite X/AC Composites. *J Chem (Hindawi, Online)* 2019;2019:13–4.

57. Pino D, Bessieres D. CH_4/CO_2 Mixture Adsorption on a Characterized Activated Carbon. *Journal of Chemical & Engineering Data* 2017;62(4):1475–80. URL: http://pubs.acs.org/doi/10.1021/acs.jced.6b01029. doi:10.1021/acs.jced.6b01029.

58. Heuchel M, Davies GM, Buss E, Seaton NA. Adsorption of Carbon Dioxide and Methane and Their Mixtures on an Activated Carbon: Simulation and Experiment. *Langmuir* 2002;15(25):8695–705. doi:10.1021/la9904298.

59. Goetz V, Pupier O, Guillot A. Carbon dioxide-methane mixture adsorption on activated carbon. *Adsorption* 2006;12(1):55–63. doi:10.1007/s10450-006-0138-z.

60. Pino D, Plantier F, Bessieres D. Experimental determination of the adsorption isotherms in gas mixtures under extended pressure and temperature range. *Journal of Thermal Analysis and Calorimetry* 2014;117(3):1469–77. doi:DOI10.1007/s10973-014-3931-z.

61. Durán I, Álvarez-Gutiérrez N, Rubiera F, Pevida C. Biogas purification by means of adsorption on pine sawdust-based activated carbon: Impact of water vapor. *Chemical Engineering Journal* 2018;353(July):197–207. URL: https://doi.org/10.1016/j.cej.2018.07.100. doi:10.1016/j.cej.2018.07.100.

62. Cracknell RF, Nicholson D, Tennison SR, Bromhead J. Adsorption and selectivity of carbon dioxide with methane and nitrogen in slit-shaped carbonaceous micropores: Simulation and experiment. *Adsorption* 1996;2(3):193–203. doi:10.1007/BF00128301.

63. Xia Y, Zhu Y, Tang Y. Preparation of sulfur-doped microporous carbons for the storage of hydrogen and carbon dioxide. *Carbon* 2012;50(15):5543–53. URL: http://dx.doi.org/10.1016/j.carbon.2012.07.044. doi:10.1016/j.carbon.2012.07.044.

64. Seema H, Kemp KC, Le NH, Park SW, Chandra V, Lee JW, Kim KS. Highly selective CO_2 capture by S-doped microporous carbon materials. *Carbon* 2014;66:320–6. URL: http://dx.doi.org/10.1016/j.carbon.2013.09.006. doi:10.1016/j.carbon.2013.09.006.

65. Fatemi S, Vesali-Naseh M, Cyrus M, Hashemi J. Improving CO_2/CH_4 adsorptive selectivity of carbon nanotubes by functionalization with nitrogen-containing groups. *Chem Eng Res Des* 2011;89(9):1669–75. URL: http://dx.doi.org/10.1016/j.cherd.2010.10.002. doi:10.1016/j.cherd.2010.10.002.

66. Bacsik Z, Cheung O, Vasiliev P, Hedin N. Selective separation of CO_2 and CH_4 for biogas upgrading on zeolite NaKA and SAPO-56. *Applied Energy* 2016;162:613–21. doi:10.1016/j.apenergy.2015.10.109.

67. Rios RB, Stragliotto FM, Peixoto HR, Torres AEB, Bastos-Neto M, Azevedo DCS, Cavalcante Jr CL. Studies on the adsorption behavior of CO_2-CH_4 mixtures using activated carbon. *Brazilian Journal of Chemical Engineering* 2013;30(4):939–51. URL: http://www.scielo.br/scielo.php?script=sci{_}arttext{&}pid=S0104-66322013000400024{&}lng=en{&}tlng=en. doi:10.1590/S0104-66322013000400024.

68. Dreisbach F, Staudt R, Keller JU. High pressure adsorption data of methane, nitrogen, carbon dioxide and their binary and ternary mix-

tures on activated carbon. *Adsorption* 1999;5(3):215–27. doi:10.1023/A:1008914703884.

69. Ribeiro RP, Sauer TP, Lopes FV, Moreira RF, Grande CA, Rodrigues AE. Adsorption of CO $_2$, CH_4 , and N_2 in Activated Carbon Honeycomb Monolith. *Journal of Chemical & Engineering Data* 2008;53(10):2311–7. URL: https://pubs.acs.org/doi/10.1021/je800161m. doi:10.1021/je800161m.

70. Yuan B, Wu X, Chen Y, Huang J, Luo H, Deng S. Adsorption of CO_2, CH_4, and N_2 on Ordered Mesoporous Carbon: Approach for Greenhouse Gases Capture and Biogas Upgrading. *Environmental Science & Technology* 2013;47(10):5474–80. URL: http://pubs.acs.org/doi/10.1021/es4000643. doi:10.1021/es4000643.